LJS Vol. 27, No. 02 (2024) 96-106

The Libyan Journal of Science
University of Tripoli Vol. 27, No. 02
https://uot.ed.ly/journals/index.php/ljs

Synthesis, structure analysis, and optical parameters investigation of Zirconium dioxide nanoparticles pure and dispersed in poly(vinylpyrrolidone) nanocomposite

Abdulhakim A. Jangher*[1], Abdullah H. Almokhter[2], Ali Ben Ahmed[3]

1.University of Tripoli, Faculty of Sciences, Departments of Chemistry, Tripoli, Libya.

2.The Libyan Academy, School of Basic Sciences, Department of Chemistry, Tripoli, Libya.

3.University of Sfax, Faculty of Sciences of Sfax, Department of Physic, Sfax, Tunisia.

Corresponding author: Abdulhakim A. Jangher a.jangher@uot.edu.ly

ARTICLE INFO

Article history:

Received 20/07 /2024

Received in revised form 11/ 08 /2024

Accepted 21 /08 /2024

ABSTRACT

Poly(vinylpyrrolidone), PVP is used in several potential applications, based on its particular chemical and physical properties. The objective of this work is to prepare PVP-zirconium dioxide, (PVP-ZrO_2) nanocomposites. ZrO_2 NPs were obtained by the sol-gel method. The formation of spherical ZrO_2 NPs, PVP film, and PVP-ZrO_2 nanocomposites was characterized using X-ray diffraction (XRD), Fourier transform infrared spectroscopy (FTIR), and optical spectroscopy (UV-visible and Fluorescence). The XRD patterns revealed the monoclinic crystal structure of the ZrO_2 NPs (average size of 19 nm) and the successful doping operation. The FT-IR spectra revealed the strong interaction between the PVP polymer and the ZrO_2. The absorption edges of all nanocomposites shifted to the higher wavelength region compared to the pure polymer. The results indicate that the optical bandgap values decreased as the ZrO_2 content increased. Additionally, from pure PVP to nanocomposites by different concentrations, the emission peak broadens towards the higher wavelength side, with offset superiority for 5% ZrO_2 NPs/PVP nanocomposite. All these results indicate the eligibility of the ZrO_2NPs/PVP blend nanocomposites for different optoelectronic applications.

Keywords: PVP, ZrO_2, Nanocomposite, Optical parameters, Fluorescence.

1. Introduction

Nanotechnology is an active field; it is in a phase of rapid progress with its applications at the nanometric scale. For this, the need to design new materials with improved properties has forced the rapid development

of nanomaterials. Nanoparticles possess unique physicochemical, optical, and biological properties that can be appropriately manipulated for desired applications in various fields such as medical and biomedical, optical and optoelectronic devices, and solar cells [1-8]. Zirconium dioxide (ZrO_2), is an important metal oxide. Zirconium dioxide nanoparticles (ZrO_2 NPs) have been widely used in a variety of applications [9-19]. The usefulness of ZrO_2 nanoparticles depends on their size and their interesting physical properties. ZrO_2 NPs will be synthesized employing various methods like sol-gel [20], combustion [21], hydrothermal [22], co-precipitation[23], and green [24]. Polyvinylpyrrolidone (PVP) is a polymer with many interesting physical properties. Various optoelectronic applications [25-27] require materials with improved structural, electrical, and optical properties. The development of new nanodevices requires the manufacture of nanocomposites formed by pure polymers (such as PVP) doped with inorganic materials having nanometric sizes such as nanoparticles of Zirconium dioxide (ZrO_2). ZrO_2 is a semiconductor, flexible has good moldability, and has interesting optical and dielectric properties.

In the present work, ZrO_2 nanoparticles (NPs) have been synthesized using the sol-gel method and ZrO_2/PVP composite films with different concentrations of ZrO_2 NPs. All samples were characterized and analyzed by XRD, FT-IR, UV-Vis, and Fluorescence spectroscopies. The effect of ZrO_2 NPs concentration on the optical properties of PVP films will also be analyzed and discussed.

2. Materials and methods

2.1. nthesis of zirconium dioxide nanoparticles

Nanoparticles of ZrO_2 were prepared using the sol-gel method. The proper amounts of 0.2 M zirconyl chloride octahydrate, ($ZrOCl_2.8H_2O$) as a metal precursor, (6.45 g) were dissolved in 100 ml distilled water put in a beaker of 250 mL and 2.0 M of ammonium hydroxide (NH_4OH). The ammonium hydroxide was titrated drop by drop with zirconyl chloride solution with magnetic stirring for 2 h to obtain a good homogeneity. Measured pH ≈ 9-10. The white gel was filtered with Whitman No.1. filter paper by air vacuum pump with reassign washing the gel three times with double distilled water and put in the oven for dry at 110^{o}C for about 2 h, finally calcined the gel at a temperature of 600 ^{o}C about 3 h to obtain zirconium dioxide nanoparticles [28, 29].

2.2. Fabrication of zirconium dioxide-loaded PVP nanocomposite films

By solution casting technique, PVP/ZrO_2 the nanocomposites were prepared. In the composition, 5%, 10%, and 20% ZrO_2 NPs were added to the aqueous solution of PVP. To obtain the nanocomposite films, the mixtures are left to dry in a clean room at room temperature.

2.3. Characterization techniques

ZrO_2 NPs and PVP/(0%, 5%, 10%, 20%)ZrO_2 nanocomposites were characterized by X-ray diffraction, XRD, FT-IR, UV-Vis, and fluorescence spectroscopies

3. Results and discussions

3.1. Structure description

The XRD pattern of ZrO_2 powder is shown in Figure 1. The XRD spectrum clearly shows the crystalline structure of the nanoparticles and various peaks of ZrO_2. The XRD pattern shown in Figure 1 has crystalline diffraction peaks at 2θ values of 29.48^o, 42.58^o, 51.41^o, 57.95^o, 65.53^o, and 70.02^o corresponding to (-111), (211), (101), (-221), (130), (-231), and (140) planes, respectively, of monoclinic ZrO_2 (ICDD File No. 37-1484).

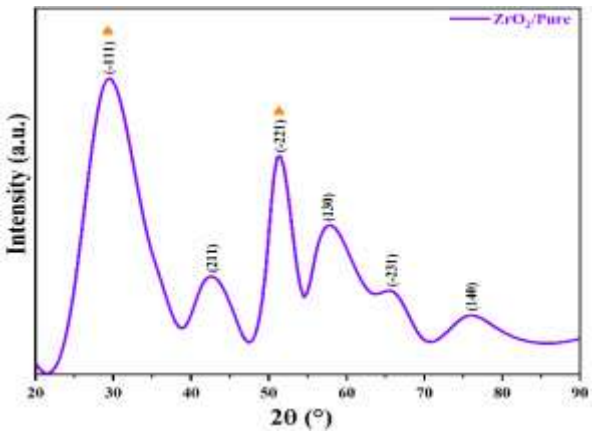

Fig.1. XRD patterns of pure ZrO_2 NPs

The average crystallite size (*D*) of ZrO_2 NPs is deducted from the Scherrer formula [30]. The average crystallite size of nanoparticles (*D*) is equal to 19 nm. XRD pattern of functionalized PVP with ZrO_2 NPs of 5, 10, or 20 wt % is shown in Figure 2. PVP has a peak at 2θ = 22.6°, this peak is characterized for PVP, and this is in good agreement with results reported in the literature [31]. The XRD pattern of PVP-ZrO_2 nanocomposites films showed two peaks at 2θ = 28.6°, and 2θ = 49.6° corresponding to the ZrO_2 NPs, with a shift compared to pure ZrO_2. This is due to the effect of the interaction of ZrO_2 NPs with the polymer PVP. The FT-IR spectrum of the sample of synthesized ZrO_2 NPs is given in Figure 3.

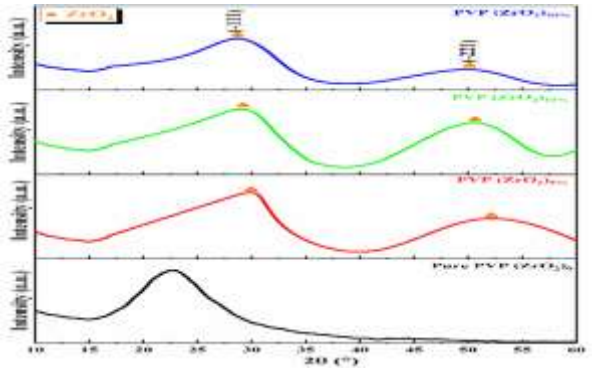

Fig.2. XRD patterns of pure PVP and ZrO_2 NPs doped PVP (5%, 10%, and 20%)

The band at 1432 cm^{-1} is due to Zr-O-Zr asymmetric stretching. The band at 960 cm^{-1} and 879 cm^{-1} are due to Zr-O stretching. This conforms to the formation of ZrO_2. The broad peak shows that the particles have nanostructure. Figure 4 Illustrate the FT-IR spectrum of PVP/ZrO_2 nanocomposites and pure PVP. The result confirmed the formation of PVP/ZrO_2 nanocomposites. A wide band appeared at 3441 cm^{-1} due to OH stretching vibration. A middle peak and a weedy shoulder showed at 2944 cm^{-1} and 2888 cm^{-1}, which correspond to symmetric and asymmetric stretching vibrations of CH_2, respectively. A sharp peak attributed to C=O stretching vibration appeared at 1650 cm^{-1}, followed by a medium peak at 1419 cm^{-1} which could be assigned to the scissoring vibration of the CH_2 group. C–N stretching appeared at 1275 cm^{-1}. CH_2 twisting vibration appeared at 1068 cm^{-1}. Comparing with PVP spectrum, and which may be due to the small amount of ZrO_2 NPs present in the samples, the spectra of PVP–ZrO_2 nanocomposites showed a medium shift. These results in good agreement with the results obtained from XRD.

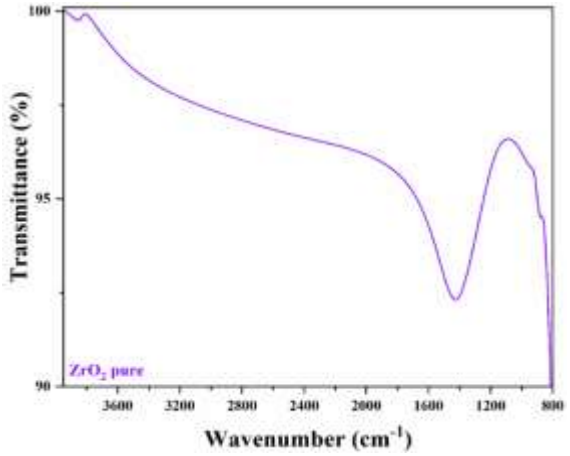

Fig. 3. FT-IR spectrum of ZrO_2 pure

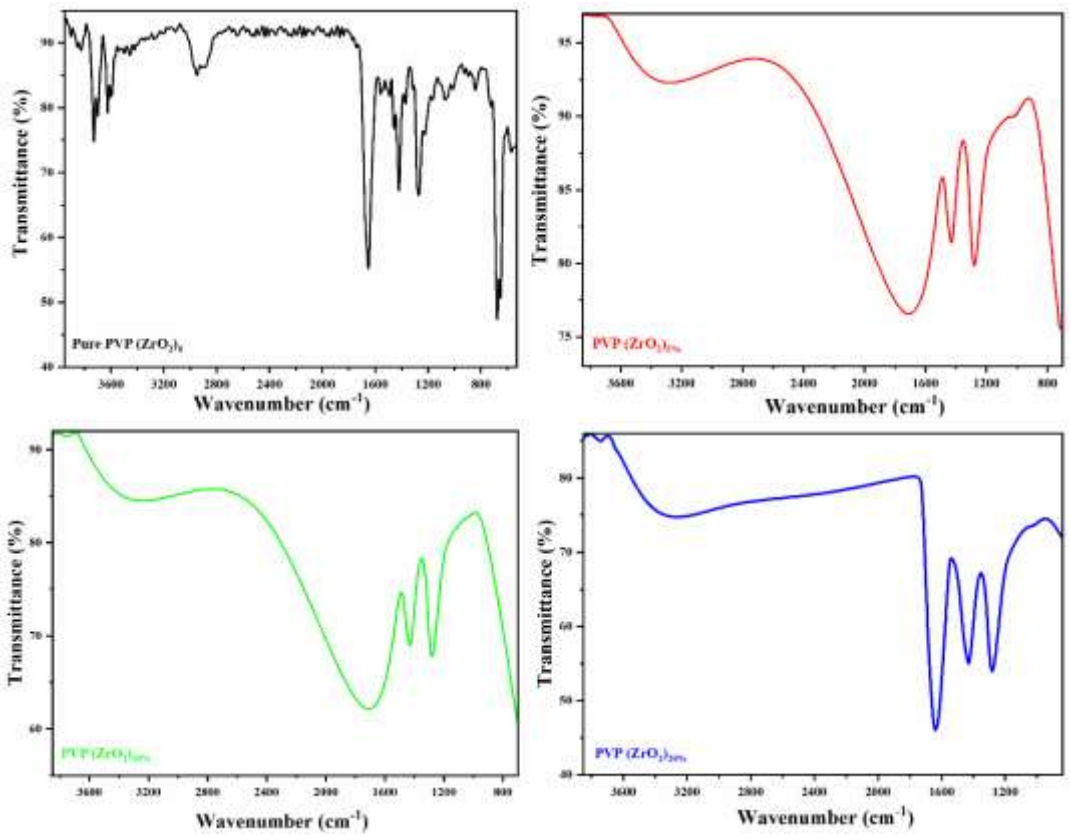

Fig.4. FT-IR spectra of PVP pure, and ZrO_2 NPs doped PVP (5%, 10%, and 20%)

3.2. UV-visible absorption spectra and optical bandgap analysis

The optical absorption spectrum of ZrO_2 NPs is shown in Figure 5. As can be seen in Figure 5, the absorption spectrum shows one strong distinguished band, and one medium band centered at λ_1 (306 nm) and λ_2 (257 nm), respectively. The strong absorption band at λ_1 was attributed to an electronic transition between O (2p) states and the Zr (4d) states. This band confirms the presence of monoclinic ZrO_2 NPs. This result is close to the values reported in the previously published literature [32, 33]. The weak absorption band at λ_2 was probable due to the defect states or impurities [34, 35]. The UV-visible absorption spectrum of pristine PVP was shown in Figure 6. As it can be seen the spectrum of PVP film reveals a strong peak centered at 305 nm.

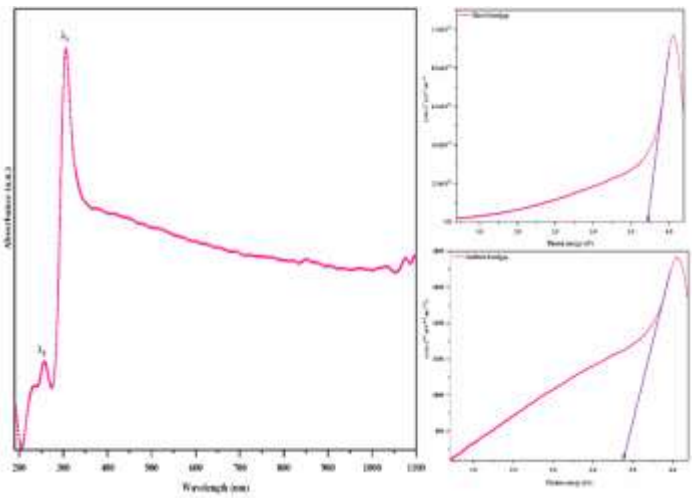

Fig.5. UV-visible absorption spectrum and energy band gap determination plot of pure ZrO_2 NPs

The absorption spectra for varying doping percentages of ZrO_2 in the PVP matrix in the wavelength range of 190 -1100 nm have been shown in Figure 6. The

absorption edges of all nanocomposites shifted to the higher wavelength region compared to the pure region. The nanocomposites showed a broad absorption peak at 305-311 nm. In the UV region, the spectra show a systematic shift of the maximum absorption to higher wavelengths. The addition of ZrO_2 nanoparticles to the composite resulted in a noticeable increase in absorbance values, indicating a strong interaction between the nanoparticle and the host polymer matrix. For the highest concentration of ZrO_2 NPs (20%), the maximum absorbance wavelength starts to decrease as samples with high ZrO_2 content reach the maximum absorbance values of the spectrophotometer. ZrO_2NPs are known for their high refractive index, and at higher concentrations, scattering effects can become prominent. This scattering can shift the apparent absorbance peak or reduce the intensity of light reaching the detector, potentially skewing the data toward lower wavelengths. At higher concentrations, interactions between the nanoparticles (such as aggregation) may alter their optical properties, leading to a shift in the maximum absorbance wavelength.

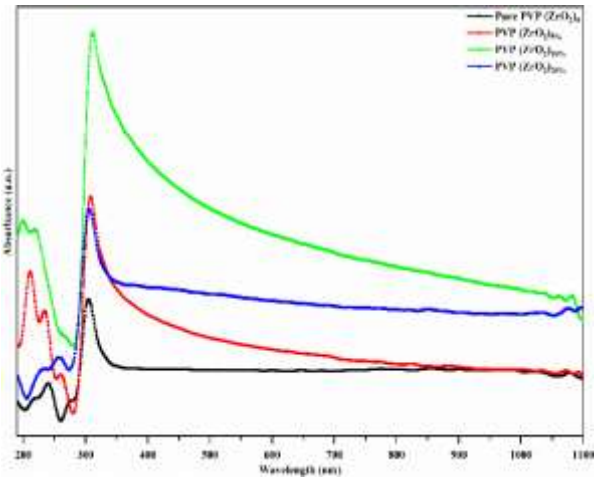

Fig.6.UV-Visible absorption spectra of PVP pure, and doped with different % ZrO_2

By applying Beer-Lambert's law [36], Figure 7 indicates that the steepness of the absorption coefficient curve increases with the increases of ZrO_2 concentration in the nanocomposites from pure $PVP(ZrO_2)_0$ to $PVP(ZrO_2)_{20\%}$. As can be seen in Figure 8, by increasing the ZrO_2-dopant concentration from 0 to 10 %, the k-values increased because the optical absorption for those composites is improved. While, by increasing the ZrO_2 dopant concentration to 20%, the k-values decreased because the optical absorption for this composite is degraded. This result has been observed in previous works [37- 39].

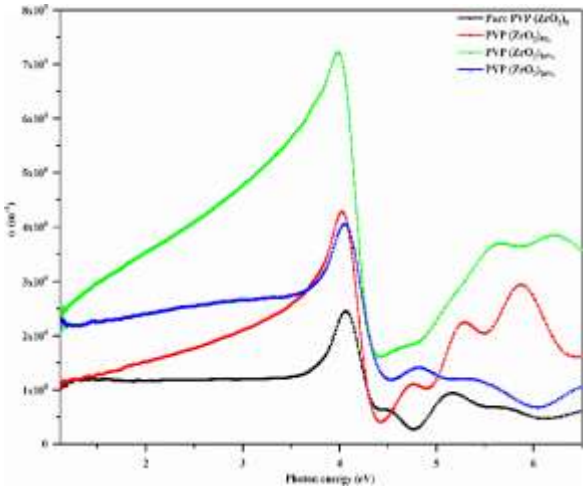

Fig. 7. Optical absorption coefficient versus photons energy for PVP pure and doped with different %ZrO_2

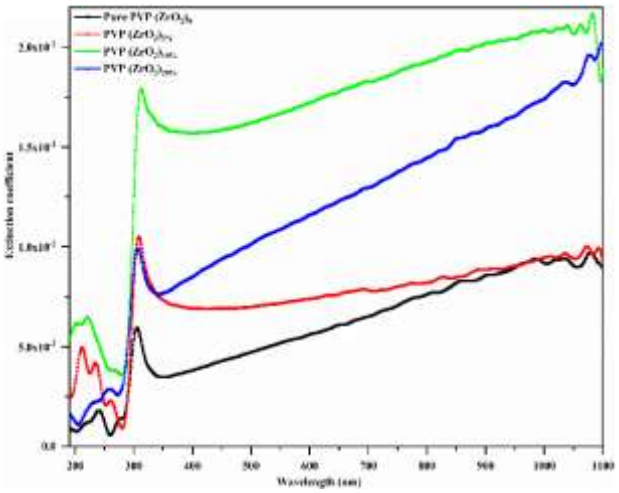

Fig. 8. Variation of extinction coefficient as a function of wavelength for PVP pure, and doped with different % ZrO_2

The band gap energy of the ZrO_2 NPs was estimated from the optical absorption spectrum through Tauc plots (Figure 5). The direct and indirect band gap of the prepared ZrO_2 NPs is about 3.72 eV, and 3.38 eV, respectively. The energy band gap of ZrO_2 NPs as a wide band gap insulator varies between 3.0 to 5.7 eV [40-42]. The band gap energy values of the nanocomposite decreased as the ZrO_2 content increased. This decrease is attributed to the effect of the ZrO_2 on the PVP, particularly at 10% content (see Figure 9 (a, b), and Table 1). Specifically, the direct energy bandgap (E_{gd}) decreased from 3.79 eV to 3.36 eV for the PVP ZrO_2 nanocomposite films. However, there was the sale significant difference in the indirect energy bandgap (E_{gind}), which decreased from 3.51 eV to 2.38 eV. This is explained by the creation of new band levels, allowing electronic transitions from the valence band to the conduction band, which reduces the width of the bandgap.

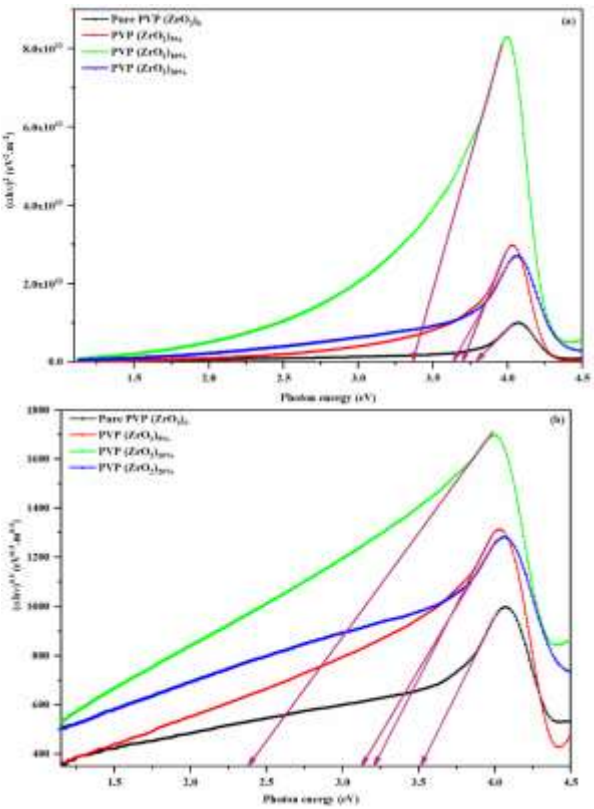

Fig.9. Direct (a) and indirect (b) optical band gap energies for PVP pure, and doped with different % ZrO_2

Table .1. Direct and indirect optical bandgap for (ZrO_2, PVP) pure and PVP doped with different %ZrO_2

Samples	E_{gd} (eV)	E_{gind} (eV)	λ_{max}(nm)
Pure ZrO_2	3.72	3.38	306
PVP(ZrO_2)$_0$	3.79	3.51	305
PVP(ZrO_2)$_{5\%}$	3.7	3.2	309
PVP(ZrO_2)$_{10\%}$	3.36	2.38	311
PVP(ZrO_2)$_{20\%}$	3.63	3.12	306

3.3. Fluorescence properties

The fluorescence spectra of ZrO_2 NPs, PVP pure, and nanocomposites content when the excitation wavelength was 375 nm in the wavelength range of 400 nm to 750 are shown in Figures. (10, 11). As can be seen Figure 10, the fluorescence spectrum of ZrO_2 NPs showed a wide fluorescence band from 400 nm to 750 nm. The maximum fluorescence intensity was detected in the region [585- 690nm]. The corresponding CIE coordinates is (0.4350, 0.4410), which constitutes a triangular region in the neighborhood of the equienergy point of white light (0.33, 0.33) in the CIE chromaticity diagram. Pure PVP shows wide emission peak centered at 480 nm. However, the ZrO_2 NPs/PVP nanocomposite reveals wide emission peaks from (568 nm to 710 nm) due to incorporating ZrO_2 NPs into the PVP. From pure PVP to nanocomposites by different concentrations, the emission peak extends on the road to the higher wavelength side, with offset superiority for 5% ZrO_2 NPs/PVP nanocomposite. According to the CIE color map (Figure 11), all nanocomposites emit an orange, yellow, and green color, for (5%, 10%, and 20%) ZrO_2 NPs/PVP, respectively (see Table 2). According to these results, the prepared nanocomposites are potential candidates for various optoelectronic applications [43-46].

Table .2. Color coordinates, and dominant wavelength of the pure PVP, pure ZrO_2, and PVP doped with different % ZrO_2

Samples	CIE coordinates	Dominant wavelength
ZrO_2	(0.4350,0.4410)	577 nm → Yellow
$PVP(ZrO_2)_0$	(0.1745,0.1931)	479 nm → Blue
$PVP(ZrO_2)_{5\%}$	(0.6538,0.3459)	606 nm → Orange
$PVP(ZrO_2)_{10\%}$	(0.4657,0.5042)	575 nm → Yellow
$PVP(ZrO_2)_{20\%}$	(0.3752,0.4728)	565 nm → Green

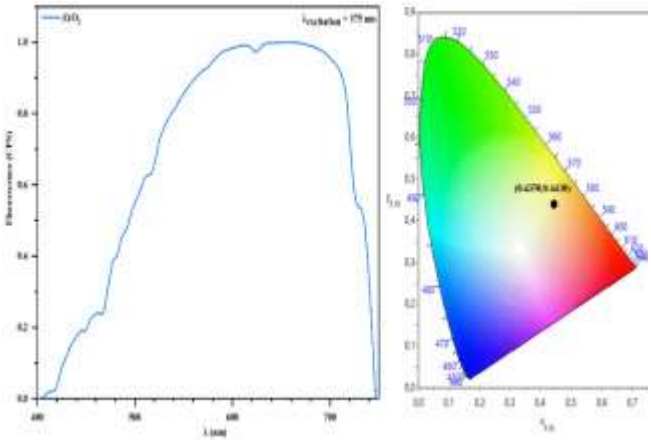

Fig.10. Fluorescence emission spectrum and CIE coordinates of pure ZrO_2 NPs

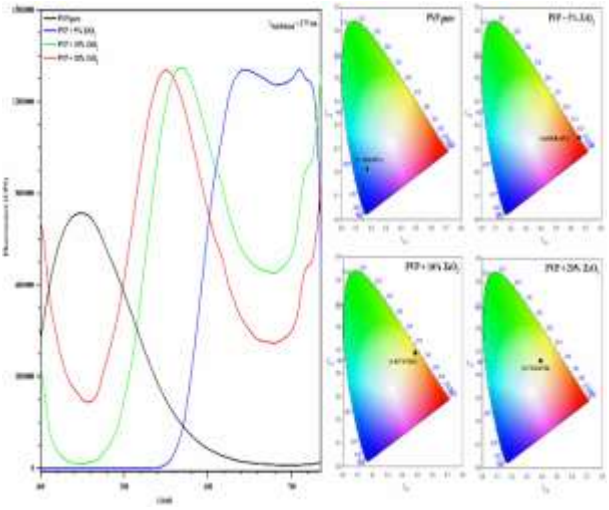

Fig.11. Fluorescence emission spectra and CIE coordinates for PVP pure, and doped with different % ZrO_2

4. Conclusion

The synthesis and characterization of PVP/ZrO_2 nanocomposites through the simple casting method reveal significant insights into their structural and optical properties. The monoclinic structure of zirconium dioxide (ZrO_2) is confirmed via X-ray diffraction (XRD), and the incorporation of ZrO_2 nanoparticles (NPs) into the polyvinylpyrrolidone (PVP) matrix is verified. As the concentration of ZrO_2 increases, the optical band gap narrows from 3.79 eV to 3.36 eV, demonstrating tunability in optical properties depending on ZrO_2 content.

Moreover, the absorption and extinction coefficients, which are important for optoelectronic applications, rise with higher ZrO_2 content. The study also notes that the prepared nanocomposites exhibit emissions in the orange, yellow, and green color ranges, further supporting their potential for use in optoelectronic devices. The color emission variation due to different ZrO_2 concentrations enhances their suitability for applications such as light-emitting devices or sensors.

These characteristics suggest that PVP/ZrO_2 nanocomposites hold promise in advancing the development of optoelectronic components where tunable optical properties and color emissions are critical.

5. Acknowledgments

The authors wish to thank engineer Wedad Alakrash for her help in conducting some experiments FT-IR, Engineer Mohamed Tarface from Petroleum Research Center (PRC) for supplying XRD, Prof. S. K. Shahooki for his help, Department of Chemistry, Faculty of Science, Tripoli University and Dr. A. B. Ahmed, Department of Physic, Faculty of Sciences of Sfax, University of Sfax, Sfax, Tunisia for conducting UV-Visible absorption measurements.

6. References

[1] E. Mansfield, D. L. Kaiser, D. Fujita , M. Van de Voorde. Nanomaterials for Energy Applications. Wiley **(2017).** https://doi.org/10.1002/9783527800308.ch28

[2] H. Wang, X. Liang, J. Wang, Sh. Jiao, D. Xue. Multifunctional inorganic nanomaterials for energy applications. Nanoscale. 12 (2020) 14-42. https://doi.org/10.1039/C9NR07008G

[3] J. W. M. Bulte, M. M. J. Modo. Design and Applications of Nanoparticles in Biomedical Imaging. Springer **(2017)**. Design and Applications of Nanoparticles in Biomedical Imaging | SpringerLink

[4] H. Ahmed, A. Hashim. Design and Tailoring the Optical and Electronic Characteristics of Silicon Doped PS/SnS_2 New Composites for Nano-Semiconductors Devices. Silicon. 14 **(2022)** 6637-6643. https://doi.org/10.1007/s12633-021-01449-x

[5] V. Torres-Costa. Nanostructures for Photonics and Optoelectronics. Nanomaterials. 12 **(2022)** 1820. https://doi.org/10.3390/nano12111820

[6] G. M. Abdelghani, A. Ben Ahmed, A. B. Al-Zubaidi. Synthesis, characterization, and the influence of energy of irradiation on optical properties of ZnO nanostructures. Scientific Report. 12 **(2022)** 20016. https://doi.org/10.1038/s41598-022-24648-x

[7] I. A. Mohammed Ali, H. I. AL-Ahmed, A. Ben Ahmed. Evaluation of Green Synthesis (Withania somnifera) of Selenium Nanoparticles to Reduce Sperm DNA Fragmentation Diabetic Mice Induced with Streptozotocin. Applied Sciences. 13 (2023) 728. https://doi.org/10.3390/app13020728

[8] M. J. Mitchell, M. M. Billingsley, R. M. Haley, M. E. Wechsler, N. A. Peppas, R. Langer. Engineering precision nanoparticles for drug delivery. Nature Reviews Drug Discovery. 20 **(2021)** 101–124. https://doi.org/10.1038/s41573-020-0090-8

[9] H. M. Shinde, T. T. Bhosale, N. L. Gavade, S. B. Babar, R. J. Kamble, B. S. Shirke, K. M. Garadkar. Biosynthesis of ZrO_2 nanoparticles from Ficus benghalensis leaf extract for photocatalytic activity. Journal of Materials Science: Materials in Electronics. 29 **(2018)**14055-14064. https://doi.org/10.1007/s10854-018-9537-7

[10] I. Uddin, A. Ahmad. Bioinspired eco-friendly synthesis of ZrO_2 nanoparticles. Journal of Materials and Environment Science. 7 **(2016)** 3068-3075.

[11] M. Zarghani, B. Akhlaghinia. Green and Efficient Procedure for Suzuki–Miyaura and Mizoroki–Heck Coupling Reactions Using Palladium Catalyst Supported on Phosphine Functionalized ZrO_2 NPs (ZrO2@ ECP-Pd) as a New Reusable Nanocatalyst. Bulletin of the Chemical Society of Japan. 89 **(2016)** 1192-1200. https://doi.org/10.1246/bcsj.20160163

[12] P. Bansal, G. Bhanjana, N. Prabhakar, J. S. Dhau, G. R. Chaudhary. Electrochemical sensor based on ZrO_2 NPs/Au electrode sensing layer for monitoring hydrazine and catechol in real water samples. Journal of Molecular Liquids. 248 **(2017)** 651-657. https://doi.org/10.1016/j.molliq.2017.10.098

[13] A. Moazami, M. Montazer. A novel multifunctional cotton fabric using ZrO_2 NPs/urea/CTAB/MA/SHP: introducing flame retardant, photoactive and antibacterial properties. The Journal of The Textile Institute. 107 **(2016)** 1253-1263. https://doi.org/10.1080/00405000.2015.1100806

[14] S. Mallakpour, A. N. Ezhieh. Polymer nanocomposites based on modified ZrO_2 NPs and poly (vinyl alcohol)/poly (vinyl pyrrolidone) blend: optical, morphological, and thermal properties. Polymer-Plastics Technology and Engineering. 56 **(2017)** 1136-1145. https://doi.org/10.1080/03602559.2016.1253741

[15] R. Gillani, B. Ercan, A. Qiao, T. J. Webster. Nanofunctionalized zirconia and barium sulfate particles as bone cement additives. International journal of nanomedicine. 5 **(2010)** 1-11.

http://www.ncbi.nlm.nih.gov/pmc/articles/pmc2819907/

[16] H. Zhang, H. Lu, Y. Zhu, F. Li, R. Duan, M. Zhang, X. Wang. Preparations and characterizations of new mesoporous ZrO_2 and Y_2O_3-stabilized ZrO_2 spherical powders. Powder technology. 227 **(2012)** 9-16. https://doi.org/10.1016/j.powtec.2012.02.007

[17] J. H. Shim, C. C. Chao, H. Huang, F. B. Prinz. Atomic layer deposition of yttria-stabilized zirconia for solid oxide fuel cells. Chemistry of Materials. 19 **(2007)** 3850-3854. https://doi.org/10.1021/cm070913t

[18] R. Ramamoorthy, P. K. Dutta, S. A. Akbar. Oxygen sensors: materials, methods, designs and applications. Journal of materials science. 38 **(2003)** 4271-4282. https://doi.org/10.1023/A:1026370729205

[19] Y. H. Su, Y. S. Lai. Performance enhancement of natural pigments on a high light transmission ZrO_2 nanoparticle layer in a water-based dye-sensitized solar cell. International Journal of Energy Research. 38 **(2014)** 436-443. https://doi.org/10.1002/er.3110

[20] A. P. Ayanwale, A. D. Cornejo, J. C. C. Gonzalez, L. F. E. Cristobal, S. Y. R. Lopez, Review of the synthesis, characterization, and application of zirconia mixed metal oxide nanoparticles, International Journal of Research-Granthalaya, **(2018)**, **6**(8), 136-145. https://doi.org/10.5281/zenodo.1403844

[21] R. Srivastava. Synthesis and characterization techniques of nanomaterials. International Journal of Green Nanotechnology. 4 **(2012)** 17-27. https://doi.org/10.1080/19430892.2012.654738

[22] S. L. Jangra, K. Stalin, N. Dilbaghi, S. Kumar, J. Tawale, S. P. Singh, R. Pasricha. Antimicrobial activity of Zirconia (ZrO_2) nanoparticles and zirconium complex. Journal of Nanoscience and Nanotechnology. 12 **(2012)** 7105-7112. https://doi.org/10.1166/jnn.2012.6574

[23] A. Esmaeilifar, S. Rowshanzamir, A. Behbahani. Hydrothermal synthesis of nano-size zirconia using commercial zirconia powder: process optimization through response surface methodology. Iranian Journal of Hydrogen and Fuel Cell. 3 **(2014)** 163-173. https://doi.org/10.22104/IJHFC.2014.97

[24] S. Balaji, B. K. Mandal, S. Ranjan, N. Dasgupta, and R. Chidambaram. Nano-zirconia-evaluation of its antioxidant and anticancer activity. Journal of Photochemistry and Photobiology. B: Biology. 170 **(2017)** 125-133. https://doi.org/10.1016/j.jphotobiol.2017.04.004

[25] B. Rozenberg, R. Tenne, Polymer-assisted fabrication of nanoparticles and nanocomposites. Progress in Polymer Science. 33 **(2008)** 40 -112. https://doi.org/10.1016/j.progpolymsci.2007.07.004

[26] S. Sarkar, E. Guibal, F. Quignard, A. K. SenGupta. Polymer-supported metals and metal oxide nanoparticles: synthesis, characterization, and applications. Journal of Nanoparticles Research. 14 (2) **(2012)** 715. https://doi.org/10.1007/s11051-011-0715-2

[27] J. Virkutyte, R. S. Varma. Green synthesis of metal nanoparticles: biodegradable polymers and enzymes in stabilization and surface functionalization. Chemical Science. 2 (5) **(2011)** 837–846. https://doi.org/10.1039/C0SC00338G

[28] A. Kołodziejczak-Radzimska and T. Jesionowski. Zinc Oxide - From Synthesis to Application: A Review. Materials. 7 **(2014)** 2833-2881. https://doi.org/10.3390/ma7042833

[29] M. Conde, K. Dakhsi, H. Zouihri, K. Abdelouahdi, L. Laanab, M. Benaissa1 and B. Jaber. Preparation of ZnO Nanoparticles without Any Annealing and Ripening Treatment. Journal of Materials Science and Engineering A. 12 **(2011)** 985-990. https://doi.org/10.17265/2161-6213/2011.12.011

[30] C. Suryanarayana. M. G. Norton. X-ray diffraction a practical approach. New York: Plenum Press (**1998**).

[31] Zyoud, S.H.; AlAbdulaal, T.H.; Almoadi, A.; Alqahtani, M.S.;Harraz, F.A.; Al-Assiri, M.S.; Yahia,I.S.; Zahran, H.Y.; Mohammed, M.I.;Abdel-wahab, M.S. Linear/Nonlinear Optical Characteristics of ZnO-Doped PVA/PVP Polymeric Films for Electronic and Optical Limiting Applications. Crystals 13 **(2023)** 608. https://doi.org/10.3390/cryst13040608

[32] Fatemeh Davara, Mohammad Reza Loghman-Estarki. Synthesis and optical properties of pure monoclinic zirconia nanosheets by a new precursor. Ceramics International 40 **(2014)** 8427–8433. https://doi.org/10.1016/j.ceramint.2014.01.052

[33] Latha Kumari, G.H. Du, W.Z. Li, R. Selva Vennila, S.K. Saxena, D.Z. Wang. Synthesis, microstructure and optical characterization of zirconium oxide nanostructures. Ceramics International 35 **(2009)** 2401–2408. https://doi.org/10.1016/j.ceramint.2009.02.007

[34] M. Salavati-Niasari, M. Dadkhah, Pure cubic ZrO2 nanoparticles by thermolysis of a new precursor, Polyhedron 28 **(2009)** 3005–3009.

[35] M. Angeles-Rosas, M. A. Camacho-López, E. Ruiz-Trejo, Structure, conductivity and luminescence of 8 mol % scandia-doped zirconia prepared by sol–gel. Solid State Ion. 181 **(2010)** 1349–1354. https://doi.org/10.1016/j.ssi.2010.07.032

[36] J. Wang, X. Deng, F. Zhang, D. Chen, W. Ding. ZnO nanoparticle-induced oxidative stress triggers apoptosis by activating JNK signaling pathway in cultured primary astrocytes. Nanoscale Research Letters 9 **(2014)** 117. https://doi.org/10.1186/1556-276X-9-117

[37] T. H. AlAbdulaal, H. E. Ali, V. Ganesh, A. M. Aboraia, Y. Khairy, H. H. Hegazy, A. V. Soldatov, H. Y. Zahran, M. S. Abdel-wahab, I. S. Yahia, Optik **(2021)**, 245, 167724, https://doi.org/10.1016/J.IJLEO.2021.167724

[38] M. S. El-Bana, S. S. Fouad. Optoelectrical properties of $Ge_{10}Se_{90}$ and $Ge_{10}Se_{85}Cu_5$ thin films illuminated by laser beams. Applied Physics A. 124, **(2018),** 132. https://doi.org/10.1007/s00339-018-1570-0

[39] H. Elhosiny Ali, M. Abdel-Aziz, A. Mahmoud Ibrahiem, Mahmoud A. Sayed, Hisham S. M. Abd-Rabboh, Nasser S. Awwad, Hamed Algarni, Mohd. Shkir, M. Yasmin Khairy. Polymers, 14 **(2022)** 1741. https://doi.org/10.3390/polym14091741

[40] M. Arakha, M. Saleem, C. Mallick Bairagi, S. Jha. The effects of interfacial potential on antimicrobial propensity of ZnO nanoparticle. Scientific Reports. 5 **(2015)** 9578. https://doi.org/10.1038/srep09578

[41] Sachin Kumar, Animesh K. Ojha. Oxygen vacancy induced photoluminescence properties and enhanced photocatalytic activity of ferromagnetic ZrO2 nanostructures on methylene blue dye under ultra-violet radiation. Journal of Alloys and Compounds 644 **(2015)** 654–662. https://doi.org/10.1016/j.jallcom.2015.04.183

[42] Sulaiman N Basahel, Tarek T Ali, Mohamed Mokhtar, Katabathini Narasimharao. Influence of crystal structure of nanosized ZrO_2 on photocatalytic degradation of methyl orange. Basahel et al. Nanoscale Research Letters **(2015)** 10:73. https://doi.org/10.1186/s11671-015-0780-z

[43] Alhulw H. Alshammari, Majed Alshammari, Khulaif Alshammari, Nageh K. Allam, T.A. Taha. PVC/PVP/SrTiO3 polymer blend nanocomposites as potential materials for optoelectronic applications. Results in Physics 44 **(2023)** 106173. https://doi.org/10.1016/j.rinp.2022.106173

[44] Jayanta Bauri, Ram Bilash Choudhary. Thermal and electronic states of exfoliated gC3N4-based nanocomposite with ZrO2 nanoparticles as a robust emissive layer. Materials Science in Semiconductor

Processing 154 **(2023)** 107205. https://doi.org/10.1016/j.mssp.2022.107205

[45] Samer H. Zyoud, Thekrayat H. AlAbdulaal, Ali Almoadi, Mohammed S. Alqahtani, Farid A. Harraz, Mohammad S. Al-Assiri, Ibrahim S. Yahia, Heba Y. Zahran, Mervat I. Mohammed, Mohamed Sh. Abdel-wahab. Linear/Nonlinear Optical Characteristics of ZnO-Doped PVA/PVP Polymeric Films for Electronic and Optical Limiting Applications. Crystals 13 **(2023)** 608. https://doi.org/10.3390/cryst13040608

[46] Nafeesah Yaqub, W.A. Farooq, M.S. AlSalhi. Delving into the properties of polymer nanocomposites with distinctive nano-particle quantities, for the enhancement of optoelectronic devices. Heliyon 6 **(2020)**e05597. https://doi.org/10.1016/j.heliyon.2020.e05597